Supplementary Information

A novel electrochemiluminescence sensor using Lu-Au@Ni-MOF for ultra-sensitive detection of permethrin

Yahui Ji, Nana You, Xiaoping Hu, Fangxin Du, Hui Gao, Jie Ru*, Gen Liu*

Key Laboratory of Green and Precise Synthetic Chemistry and Applications, Ministry of Education; Anhui Provincial Key Laboratory of Synthetic Chemistry and Applications; School of Chemistry and Chemical Engineering, Huaibei Normal University, Huaibei, Anhui 235000, P R China

* E-mail addresses: rujie@chnu.edu.cn (J. Ru); liugen7084@126.com (G. Liu)

S1. Reagents

Chloroauric acid ($HAuCl_4$), hydrochloric acid (HCl), nickel nitrate hexahydrate ($Ni(NO_3)_2 \cdot 6H_2O$), *N,N*-dimethylformamide (DMF), ethanol, and terephthalic acid (H_2BDC) were obtained from Sinopharm Chemical Reagent Co., Ltd. (China). Luminol and Nafion were purchased from Sigma-Aldrich (USA). Phosphate buffer solutions (PBS, 0.1 $mol \cdot L^{-1}$) were prepared by mixing appropriate volumes of $Na_2HPO_4 \cdot 12H_2O$ and $NaH_2PO_4 \cdot 2H_2O$ stock solutions, with the pH adjusted using 0.1 $mol \cdot L^{-1}$ H_3PO_4 or NaOH. All chemicals were of analytical grade and used as received. Ultrapure water was used throughout the experiments.

S2. Instruments

ECL measurements were performed on an ECL-9B analyzer (State Key Laboratory of Analytical Chemistry for Life Science, Nanjing University, China) equipped with a photomultiplier tube. All ECL experiments were carried out in a conventional three-electrode system: a Lu-Au@Ni-MOF modified glassy carbon electrode (GCE, 3 mm diameter) as the working electrode, an Ag/AgCl (saturated KCl) electrode as the reference electrode, and a platinum wire as the counter electrode.

The morphology and microstructure of the materials were characterized by scanning electron

microscopy (SEM, Regulus8220, Japan) and transmission electron microscopy (TEM, Jem2100UHR, Japan). X-ray diffraction (XRD) patterns were collected on a Bruker D8 Advance diffractometer (Germany) using Cu Kα radiation. Fourier-transform infrared (FT-IR) spectra were recorded on a Nicolet iS50 spectrometer (Thermo Scientific, USA). X-ray photoelectron spectroscopy (XPS) analysis was conducted on a Thermo Scientific Escalab 250Xi system (USA) with a monochromatic Mg Kα X-ray source. The specific surface area and pore size distribution of the material were determined by N_2 adsorption-desorption measurements at 77.3 K using a Micromeritics ASAP 2020 analyzer (USA), with data analyzed via the Brunauer-Emmett-Teller (BET) method and the Barrett-Joyner-Halenda (BJH) model, respectively.

S3. Preparation of ECL probes

Ni-MOF: The Ni-MOF was synthesized via a modified solvothermal method based on a reported procedure [1]. Briefly, Solution A was prepared by dissolving 2.3263 g of $Ni(NO_3)_2 \cdot 6H_2O$ in 30 mL of DMF under magnetic stirring for 30 min. Separately, Solution B was obtained by dissolving 0.6645 g of H_2BDC in 30 mL of DMF with stirring for 30 min. Solution B was then poured into Solution A, and the mixture was stirred for another 30 min while 500 μL of HCl was slowly added dropwise, yielding a homogeneous green solution. The mixture was transferred into a Teflon-lined stainless-steel autoclave and heated at 180 °C for 24 h. After cooling to room temperature, the product was collected by centrifugation at 8000 rpm, washed sequentially with DMF and anhydrous ethanol five times each, and finally dried under vacuum at 60 °C to obtain the Ni-MOF solid.

Lu-Au@Ni-MOF: The Lu-Au@Ni-MOF composite was synthesized according to a previously reported procedure with minor modifications [2]. In a typical process, 40 mg of the as-prepared Ni-MOF was dispersed in 1 mL of 10 $mmol \cdot L^{-1}$ $HAuCl_4$ solution and stirred for 4 h. Subsequently, 2 mL of 1 $mmol \cdot L^{-1}$ luminol solution was added, and the mixture was stirred for another 2 h. The resulting product was collected by centrifugation at 2000 rpm for 5 min, washed thoroughly, and finally dried under vacuum at 60 °C to obtain Lu-Au@Ni-MOF.

S4. ECL signal of GCE/Lu-Au@Ni-MOF

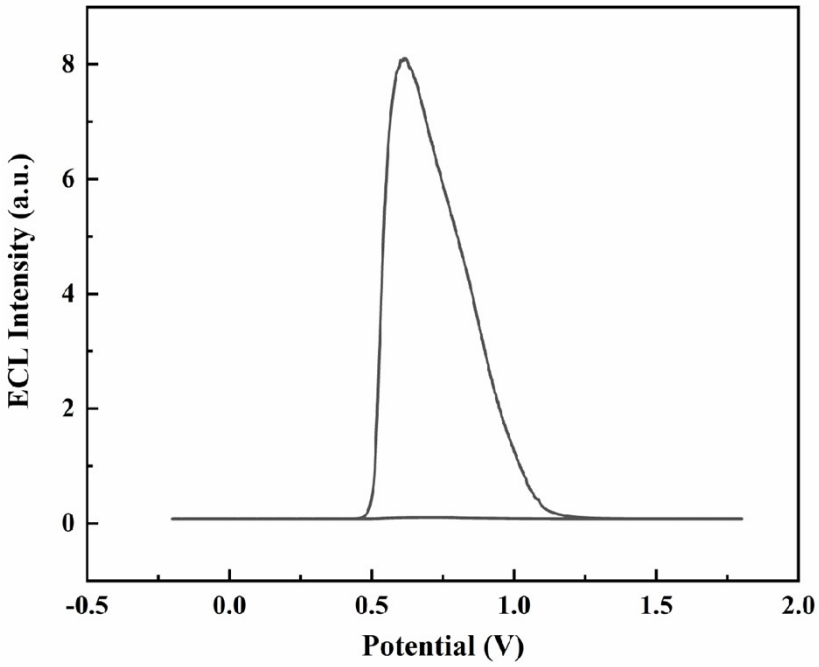

Fig. S1 ECL-potential curve of GCE/Lu-Au@Ni-MOF.

S5. EDX spectra and relative element content of Lu-Au@Ni-MOF

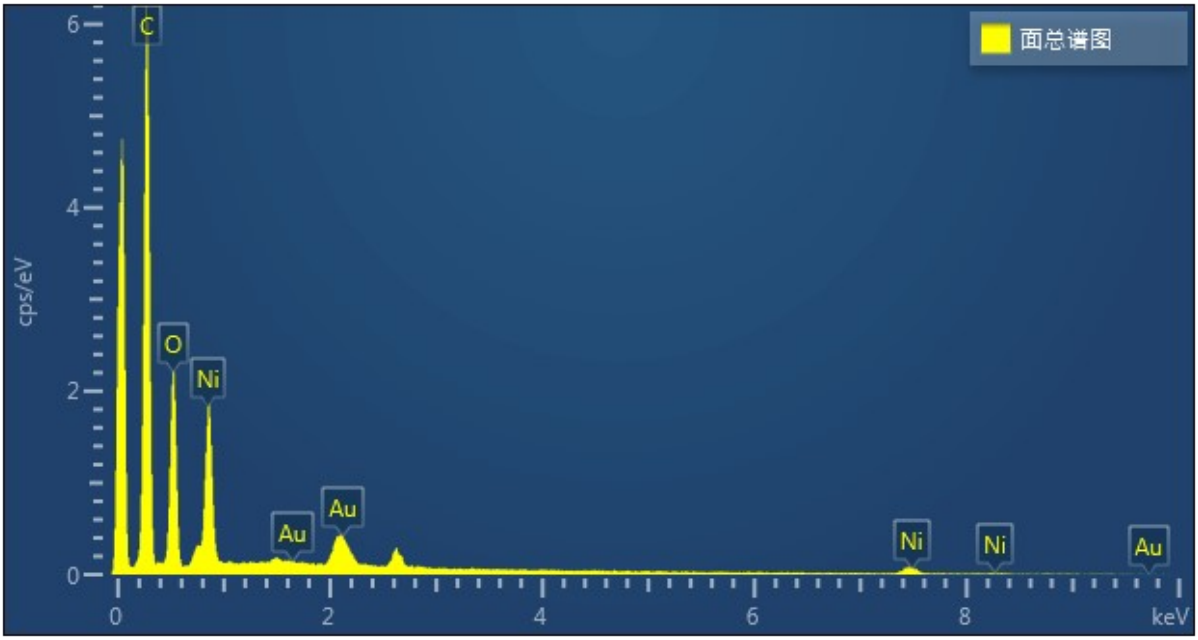

Fig. S2 EDX spectra of Lu-Au@Ni-MOF.

Table S1 SEM-EDX quantification results of Lu-Au@Ni-MOF.

Elements	Apparent concentration	k ratio	wt / %	wt / % Sigma
C K	69.72	0.69721	49.80	0.92
O K	61.69	0.20760	18.29	0.39
Ni K	62.31	0.62312	29.30	1.24
Au M	4.6	0.04597	2.61	0.37
Total			100.00	

S6. BET and BJH analysis

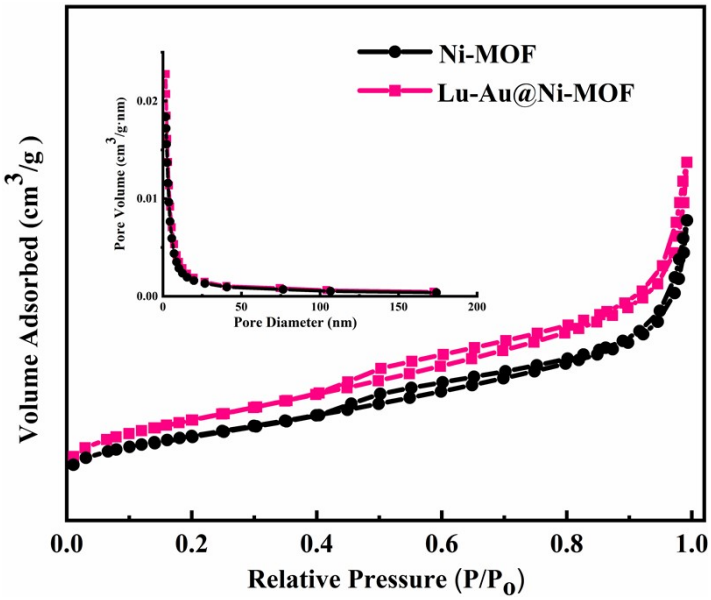

Fig. S3 N_2 adsorption-desorption isotherms and pore size distributions of Ni-MOF and Lu-Au@Ni-MOF.

Table S2 The surface area, pore volume and pore size of Ni-MOF and Lu-Au@Ni-MOF.

Samples	Surface area ($m^2 \cdot g^{-1}$)	Pore volume ($m^3 \cdot g^{-1}$)	Pore size (nm)
Ni-MOF	138.13	0.29	5.61
Lu-Au@Ni-MOF	204.10	0.37	4.86

S7. ECL response of different electrodes

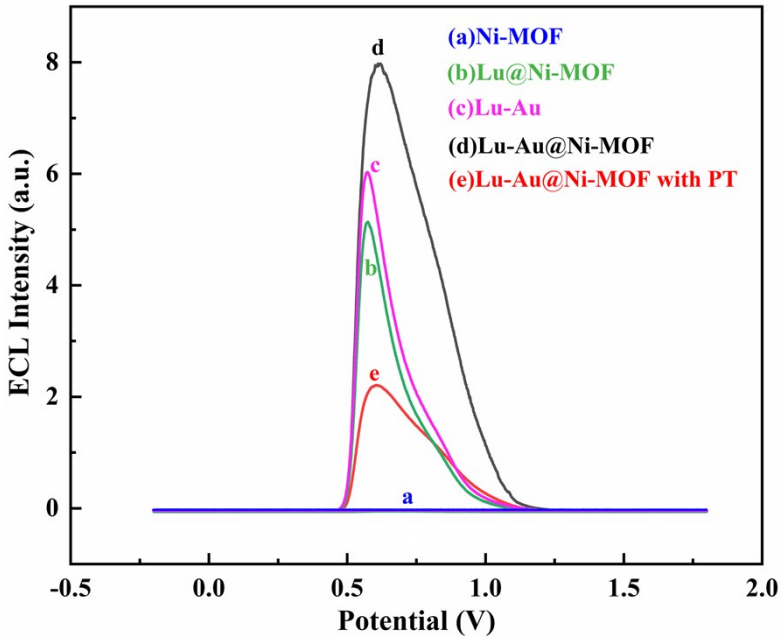

Fig. S4 ECL behavior of GCE/Ni-MOF (a), GCE/Lu@Ni-MOF (b), GCE/Lu-Au (c), GCE/Lu-Au@Ni-MOF (d), and GCE/Lu-Au@Ni-MOF with PT (e).

S8. Optimization of experimental conditions

The concentration of the co-reactant H_2O_2 is of paramount importance for the ECL efficiency. As depicted in Fig. S5, its concentration was optimized under fixed conditions (1.00×10^{-5} mol·L^{-1} PT, pH 7.0, scan rate of 100 mV·s^{-1}). The ECL intensity increased with H_2O_2 concentration from 30 to 100 mmol·L^{-1} and then plateaued. Consequently, 100 mmol·L^{-1} was chosen as the optimal concentration for subsequent experiments.

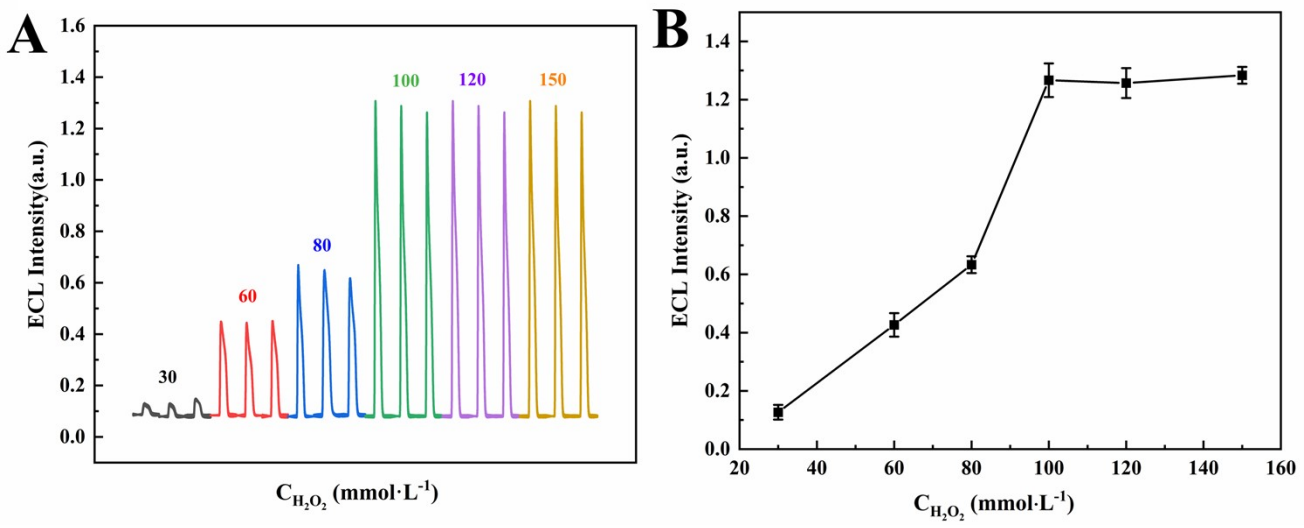

Fig. S5 (A) ECL curves of the sensor at varying H_2O_2 concentrations in the range of 30 to 150 mmol·L^{-1}; (B) The corresponding ECL intensity profiles at different H_2O_2 concentrations. The error bars represent five independent measurements.

The influence of pH on the ECL response was evaluated from 6.0 to 9.0 under fixed analytical conditions (1.00×10^{-5} mol·L^{-1} PT, scan rate of 100 mV·s^{-1}). The signal reached a maximum at pH 7.5, as illustrated in Fig. S6, and decreased on either side of this value. Accordingly, pH 7.5 was adopted for all further measurements.

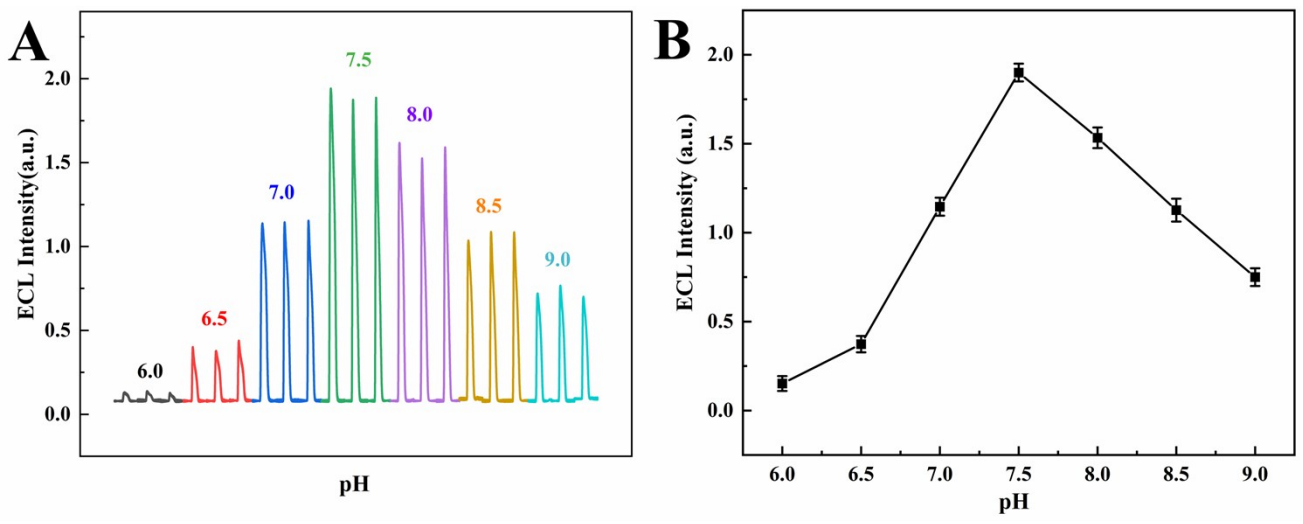

Fig. S6 (A) ECL curves of the sensor at pH 6.0 to 9.0 (pH=6.0, 6.5, 7.0, 7.5, 8.0, 8.5, 9.0); (B) the ECL changing trend diagram toward pH. The error bars represent five independent measurements.

The scan rate was optimized between 30 and 220 $mV \cdot s^{-1}$. Excessively high rates lead to signal suppression due to mass transport limitations, while overly slow rates increase measurement time and potential interference. As shown in Fig. S7, the ECL intensity increased up to 130 $mV \cdot s^{-1}$ and then decreased, establishing 130 $mV \cdot s^{-1}$ as the optimum.

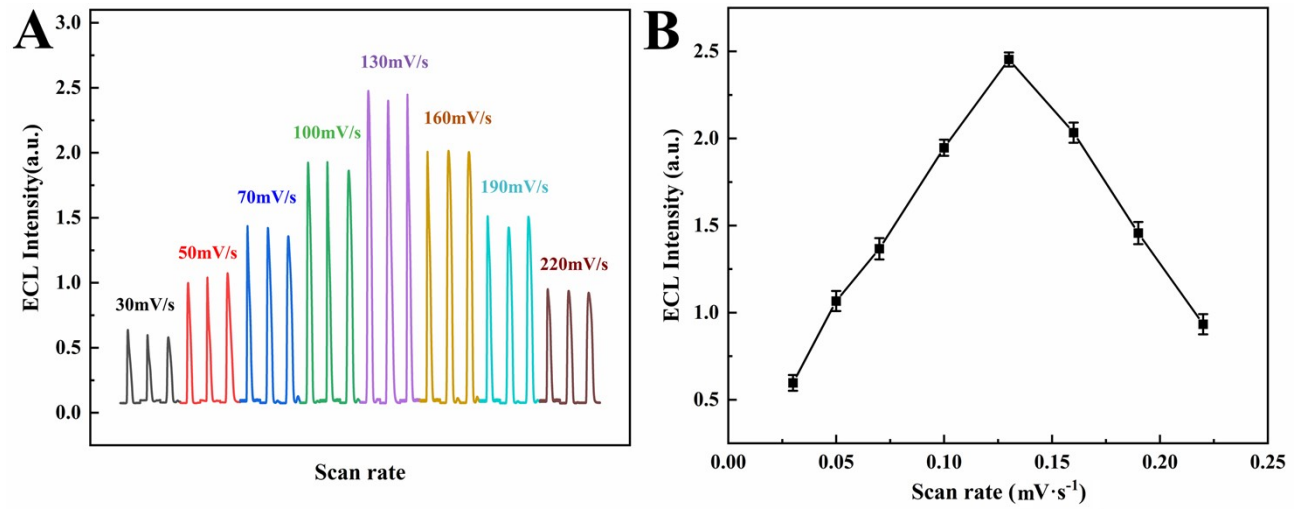

Fig. S7 (A) ECL curves of the sensor at scan rates of 30 to 220 $mV \cdot s^{-1}$; (B) the ECL changing trend diagram toward scan rates. The error bars represent five independent measurements.

S9. Comparison of different methods

Table S3 Comparison of the analytical performances of reported methods.

Methods	Linear range ($mol \cdot L^{-1}$)	LOD ($mol \cdot L^{-1}$)	Ref.
ECL	$2.60 \times 10^{-9} \sim 4.30 \times 10^{-5}$	8.70×10^{-10}	3
HPLC	$6.39 \times 10^{-8} \sim 5.11 \times 10^{-5}$	5.11×10^{-8}	4
HPLC-UV	$1.28 \times 10^{-9} \sim 2.56 \times 10^{-6}$	5.12×10^{-10}	5
SERS	$2.56 \times 10^{-7} \sim 5.12 \times 10^{-5}$	8.96×10^{-9}	6
ECL	$5.00 \times 10^{-9} \sim 5.00 \times 10^{-5}$	1.80×10^{-10}	This work

S10. PT degradation monitoring in soil

Table S4 Daily monitoring of soil PT concentration for 8 consecutive days

Day	Obtained (nmol·L^{-1})	Average	SD	RSD (%)
day 1 (reference)	81.32 73.94 75.33	76.86	3.922	5.1%
day 2	73.94 75.33 73.94	74.40	0.8025	1.1%
day 3	69.82 71.28 73.94	71.68	2.089	2.9%
day 4	65.92 69.82 68.55	68.10	1.989	2.9%
day 5	61.10 56.75 56.75	58.20	2.511	4.3%
day 6	55.59 57.81 57.54	56.98	1.211	21%
day 7	50.58 46.02 50.58	49.06	2.633	5.3%
day 8	19.58 20.73 21.58	20.63	1.004	4.9%

References

1. W. Huang, Y. Chen, L. Wu, M. Long, Z. Lin, Q. Su, F. Zheng, S. Wu, H. Li and G. Yu, Talanta, 2022, 247, 123596.
2. S. Wang, M. Wang, C. Li, H. Li, C. Ge, X. Zhang and Y. Jin, *Sensor. Actuat. B-Chem.,* 2020, 311, 127919.
3. Y. Zhao, L. Tian, S. Wu, X. Zhang, Z. Sun, Y. Hu, Y. Wang, R. Chen and J. Lu, *Microchem. J.*, 2021, 168, 106487.
4. Q. Gao, W. Liu and X. Zhu, *J. Liq. Chromatogr. R. T.*, 2020, 43, 809-818.
5. M. Pirsaheb, N. Fattahi, M. Karami and H. R. Ghaffari, *J. Food Meas. Charact.*, 2017, 12, 118-127.
6. T. B. Pham, T. H. C. Hoang, V. H. Pham, V. C. Nguyen, T. V. Nguyen, D. C. Vu, V. H. pham and H. Bui, *Sci Rep.*,2019, 9,12590.